MATERIALS SCIENCE

Direct observation of individual dislocation interaction processes with grain boundaries

Shun Kondo,[1,2] Tasuku Mitsuma,[1] Naoya Shibata,[1,3] Yuichi Ikuhara[1,2,4,5]*

In deformation processes, the presence of grain boundaries has a crucial influence on dislocation behavior; these boundaries drastically change the mechanical properties of polycrystalline materials. It has been considered that grain boundaries act as effective barriers for dislocation glide, but the origin of this barrier-like behavior has been a matter of conjecture for many years. We directly observe how the motion of individual dislocations is impeded at well-defined high-angle and low-angle grain boundaries in $SrTiO_3$, via in situ nanoindentation experiments inside a transmission electron microscope. Our in situ observations show that both the high-angle and low-angle grain boundaries impede dislocation glide across them and that the impediment of dislocation glide does not simply originate from the geometric effects; it arises as a result of the local structural stabilization effects at grain boundary cores as well, especially for low-angle grain boundaries. The present findings indicate that simultaneous consideration of both the geometric effects and the stabilization effects is necessary to quantitatively understand the dislocation impediment processes at grain boundaries.

INTRODUCTION

Plastic deformation of crystalline materials is controlled by the glide of dislocations. It is well known that dislocation glide is governed by the presence of other lattice defects (*1*). In the case of polycrystalline materials, which are used in most practical applications, dislocation glide is strongly affected by the numerous grain boundaries within the material (*2*–*4*). Thus, the influence of grain boundaries on dislocation glide is key to understanding the plastic deformation of polycrystalline materials. Among tremendous efforts to quantify such effects, the Hall-Petch relationship (*5*, *6*) has now become the basic equation to account for the effect of grain boundaries on the mechanical properties of materials. This relationship predicts that the yield stress of polycrystalline materials is inversely proportional to the square root of the average grain size; that is, the more grain boundaries there are per unit volume of a material, the stronger the material becomes. The Hall-Petch relationship has been successfully explained on the basis of a microscopic model—the so-called pileup model (*7*, *8*)—in which lattice dislocations will not easily glide through grain boundaries but instead pile up behind them. Although the Hall-Petch relationship is now widely used in designing the mechanical properties of polycrystalline materials, the origin of the pileup is still a matter of conjecture. To date, geometric and/or elastic effects [such as the continuity of slip planes in adjacent grains, the change of Burgers vectors across a grain boundary (*9*–*11*), image stress (*12*–*14*), and so on] have been mainly considered to explain the cause of the dislocation pileup at grain boundaries. However, how individual grain boundaries actually affect the motion of individual dislocations remains a long-standing question.

In recent years, in situ transmission electron microscopy (TEM) has been developed to directly observe dynamic dislocation motion in crystals under stress (*15*–*18*). In particular, in situ TEM nanoindentation techniques (*18*–*21*) allow one to dynamically observe local dislocation behavior within a TEM specimen even at the nanometer scale. Moreover, by using well-controlled bicrystals for TEM specimens (*22*–*24*), it will be possible to directly observe the interaction between dislocations and well-defined grain boundaries during deformation. Here, we show such dynamic observations of the interaction processes of individual lattice dislocations with well-defined grain boundaries in strontium titanate [$SrTiO_3$ (STO)] using in situ TEM nanoindentation techniques. Previous in situ nanoindentation research for STO single crystals (*21*) has shown that lattice dislocations with Burgers vectors of $[0\bar{1}1]$ and/or [011] on the (011) and $(0\bar{1}1)$ plane, respectively, can be introduced in a controlled manner from the indenting point when the indenter tip was inserted along the [001] direction. By further indenting the crystal, these dislocations were seen to propagate along the [100] direction. On the basis of this knowledge, we designed TEM bicrystal specimens suitable for observing the interaction between lattice dislocations and well-defined single grain boundaries.

RESULTS

In situ TEM nanoindentation for high-angle grain boundary

In situ TEM nanoindentation experiments were performed with the symmetric tilt $[010](30\bar{1})$ Σ5 grain boundary, where the rotation angle of the adjacent crystal is 36.9° (*25*, *26*). In this crystallographic orientation, the grain boundary can be considered as a model case for high-angle grain boundaries. Figure 1A shows the geometric setup of the in situ TEM nanoindentation experiments. Here, the indenter tip is of a wedge-type shape. Figure 1B shows a dark-field TEM image observed from the [010] direction before the insertion of the indenter tip. In this experiment, the indentation direction is chosen to be 18.4° inclined from the [001] direction, where the indentation direction is parallel to the grain boundary plane. The indenter tip was inserted near the grain boundary such that the lattice dislocations emitted from the indenting point would propagate to and then interact with the grain boundary. Sequential TEM images under suitable dark-field imaging conditions were recorded as a movie during the nanoindentation experiment, with a frame rate of 30 frames per second (fps).

Sequential TEM images captured from the nanoindentation movie are shown in Fig. 2. Here, we define 0 s as the starting time when the indenter tip makes contact with the specimen edge, and the time elapsed

[1]Institute of Engineering Innovation, School of Engineering, The University of Tokyo, Bunkyo, Tokyo 113-8656, Japan. [2]Center for Elements Strategy Initiative for Structural Materials, Kyoto University, Kyoto 606-8501, Japan. [3]PRESTO (Precursory Research for Embryonic Science and Technology), Japan Science and Technology Agency, Kawaguchi, Saitama 332-0012, Japan. [4]Nanostructures Research Laboratory, Japan Fine Ceramics Center, Nagoya, Aichi 456-8587, Japan. [5]WPI Advanced Institute for Materials Research, Tohoku University, Sendai, Miyagi 980-8577, Japan.
*Corresponding author. Email: ikuhara@sigma.t.u-tokyo.ac.jp

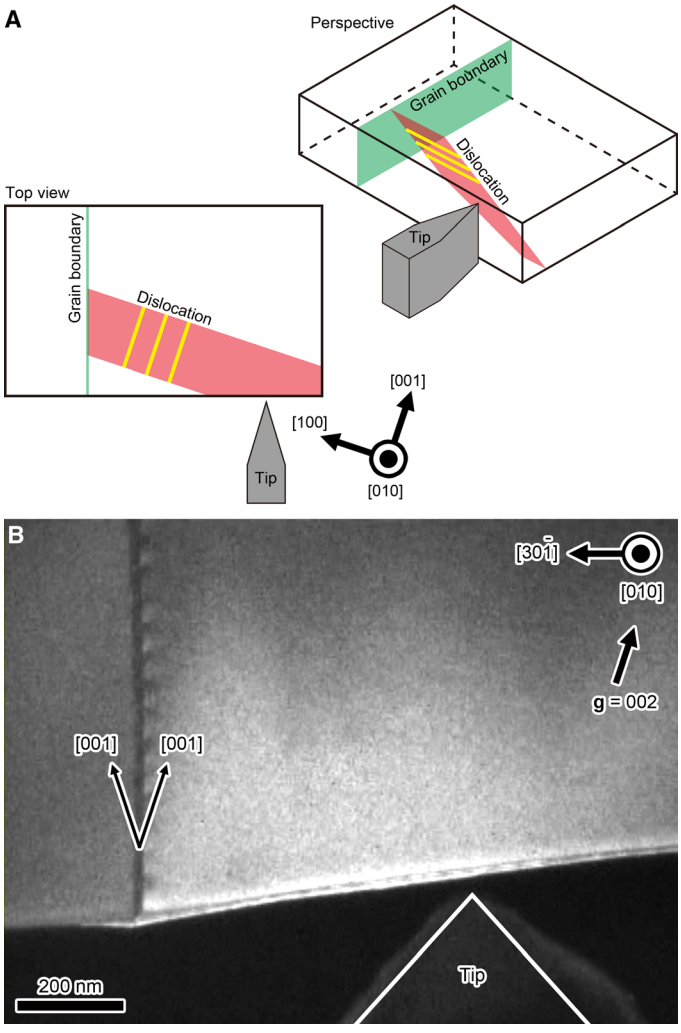

Fig. 1. TEM nanoindentation experiment for the Σ5 grain boundary. (**A**) Schematic illustration showing the geometric arrangement of the specimen, the [010](30$\bar{1}$) Σ5 grain boundary, the indenter tip, and the introduced lattice dislocation. We inserted the indenter tip into the specimen edge and observed the interaction process of the lattice dislocations with the Σ5 grain boundary. (**B**) Dark-field TEM image taken just before the nanoindentation experiment. The weak triangular contrast at the lower right is the indenter tip, and the vertical line contrast inside the specimen corresponds to the grain boundary. The indenter tip was inserted along the parallel direction to the grain boundary plane, which corresponds to the direction of 18.4° off from the [001] direction. The sample thickness is estimated to be about 300 nm.

is shown in each subsequent image. The complete real-time movie is available in the Supplementary Materials (movie S1). It is clear that the dislocations were emitted from the specimen edge and propagated along the [100] direction one by one. Using **g**·**b** dislocation contrast analyses (*27*) after the nanoindentation experiment, it was confirmed that the introduced dislocations belong to the glide system of the [0$\bar{1}$1](011) (see Supplementary Text), which is consistent with a previous report (*21*). After 19 s of continuous insertion of the indenter tip, the leading dislocation (termed the first dislocation in the image) propagated to, impinged on, and was completely attached to the grain boundary plane. The second dislocation was attached to the grain boundary plane after 26 s, and even the lower part of the third dislocation started to attach after 27 s. Other lattice dislocations following behind the third dislocation appear to pile up within the bulk crystal region. Then, the specimen edge was fractured because of the stress at the indenting point. After releasing the concentrated stress due to the fracture of the specimen edge, the intervals of dislocations were extended because of the relaxation of the repulsive forces (*1*) exerted between the dislocations with the same Burgers vector.

Dislocation impediment mechanisms at high-angle grain boundary

Our in situ observation clearly shows that the Σ5 grain boundary acts as a barrier for the lattice dislocation glide. To understand the mechanism of the impediment in detail, we first consider the effect of the geometric discontinuity across the grain boundary geometry. As illustrated in Fig. 3A, when dislocations are to cross the grain boundary, the Burgers vector has to be rotated. Because the Burgers vector must be conserved in a crystal, the rotation of the Burgers vector inevitably leaves a residual dislocation on the grain boundary plane (*9*). The Burgers vector of the residual dislocation corresponds to the difference in that of the lattice dislocation on either side of the grain boundary. The formation of the residual dislocation requires additional energy to form, which leads to an increase in the total energy. This additional energy required to form the residual dislocation makes it energetically unfavorable for the lattice dislocation to pass through the grain boundary and hence why it behaves as a barrier. Furthermore, as shown in Fig. 3B, the dislocations attached to the grain boundary during nanoindentation remain trapped, even after the external stress was removed. Thus, the grain boundary core can be an energetically stable site for dislocations. The dislocation stabilization may be caused by the dislocation dissociation on the boundary plane (*28*), elastic discontinuity (attractive image stress) (see Supplementary Text for a detailed discussion), or core structural stabilization discussed later. In any of these situations, dislocations can thus be trapped by the grain boundary core, adding another barrier to cross the grain boundary.

In situ TEM nanoindentation for low-angle grain boundary

To minimize any geometric discontinuity effects, we performed similar in situ nanoindentation experiments for a low-angle grain boundary, which is the simplest model of grain boundaries. In low-angle grain boundaries, it is well accepted that grain boundary structures can be described by a periodic array of dislocations (*29*). In the present experiments, we fabricated an STO bicrystal including the (100) low-angle tilt grain boundary with a rotation angle of 1.2° around the [010] axis. The structure of the low-angle tilt grain boundary is shown in Fig. 4A. In this case, the grain boundary structure consists of a periodic array of edge dislocations with the Burgers vector of the [100] (*30*, *31*). The interval of the edge dislocations is estimated to be about 19 nm. The TEM specimens for the in situ nanoindentation experiments are designed to effectively introduce the lattice dislocations and let them interact with the grain boundary during deformation. Figure 4B shows the geometric setup of the in situ TEM nanoindentation experiments. When considering the Burgers vector of the introduced lattice dislocations, the moving dislocations interacting with the grain boundary should be screw dislocations because the Burgers vector is parallel to the grain boundary plane. Figure 4C shows a dark-field TEM image observed from the [010] direction before the insertion of the indenter tip. The indenter tip was inserted near the grain boundary, and we dynamically observed the interaction processes between the individual lattice dislocations and the low-angle tilt grain boundary.

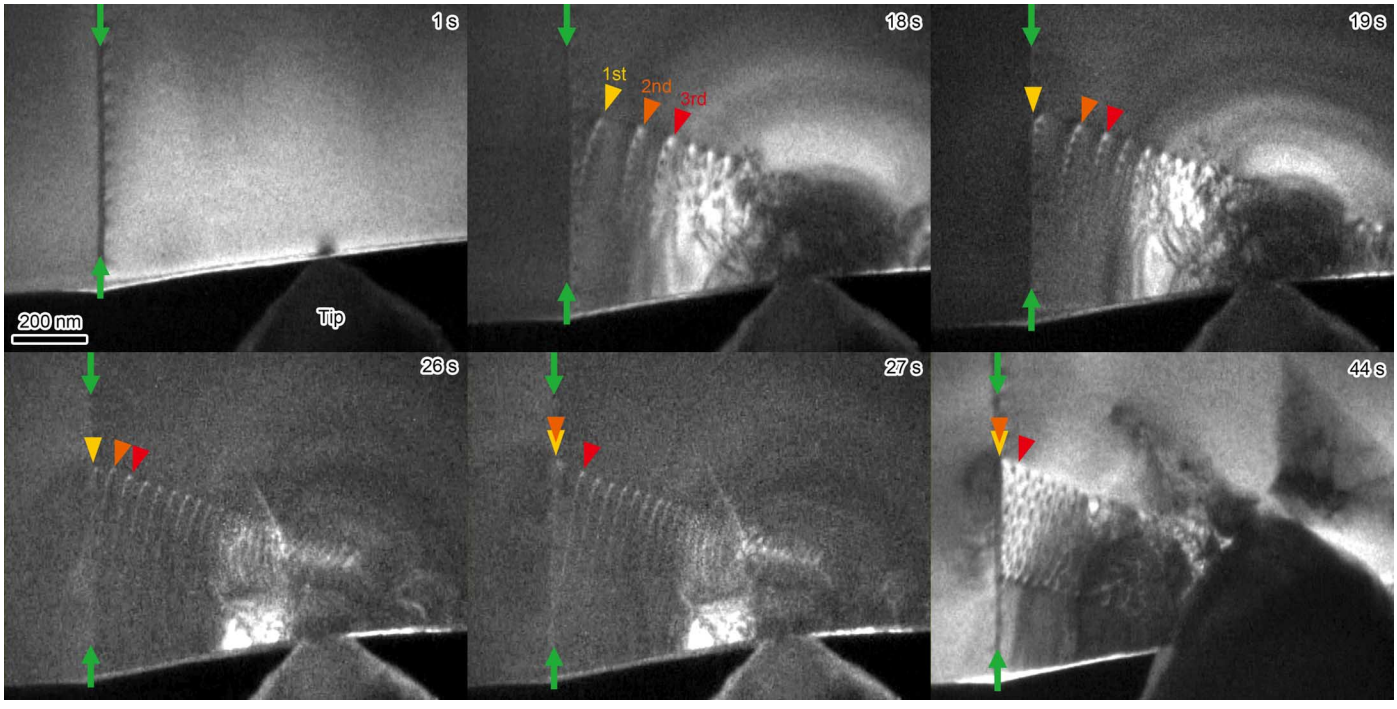

Fig. 2. Sequential TEM images captured from the movie of the nanoindentation experiment for the Σ5 grain boundary. Sequential dark-field TEM images captured from the movie recorded during the nanoindentation experiment. The line contrasts indicated by the green arrows correspond to the Σ5 grain boundary. The positions of the leading three lattice dislocations are indicated by the triangles. The indenter tip was gradually inserted from 0 to 42 s, and the specimen edge was fractured at 43 s. The dislocation motion was strongly impeded by the grain boundary, which resulted in the dislocation pileup. In this experiment, the first and second dislocations and the lower part of the third dislocation were trapped on the grain boundary plane even after the external stress was removed.

Figure 5 shows sequential TEM images captured from the movie of the nanoindentation experiment (see also movie S2). The introduced lattice dislocations have the glide system of the $[0\bar{1}1](011)$, which is confirmed by **g**·**b** contrast analyses after the nanoindentation experiment. We clearly observed that, when the indenter tip was continuously inserted, the lattice dislocations were able to traverse the grain boundary plane (see the 69 s image in Fig. 5), contrary to the Σ5 grain boundary case. However, it was found that the dislocation motion was seen to be slightly impeded at the grain boundary core region. As we extracted the indenter tip, the introduced lattice dislocations moved backward because of stress relaxation, and some dislocations crossed back over the grain boundary to the initial right-hand side crystal. During this unloading process, we again observed the grain boundary impediment effect on the lattice dislocation. Finally, one dislocation, indicated by the red arrow in Fig. 5, appeared to be caught by the grain boundary plane.

In the present low-angle tilt grain boundary case, the interaction between the lattice dislocations and the grain boundary core is actually the interaction between the lattice screw dislocations and the grain boundary edge dislocations. Figure 6A shows a dark-field image of the grain boundary edge dislocations after the crossing of the lattice screw dislocations. The dislocation lines of the grain boundary edge dislocations are seen to be shifted to the $[0\bar{1}1]$ direction, which is parallel to the Burgers vector of the lattice screw dislocations, and jogs are formed at the grain boundary dislocations. This indicates that the lattice screw dislocations intersected with the grain boundary edge dislocations during the crossing process (*32*). Because the jog length estimated from the image is much longer than the unit cell of STO, these jogs can be classified as "superjogs" (*1*). The estimated superjog length corresponds well with the product of the Burgers vector and the number of the screw dislocations crossing the grain boundary on the same glide plane (see Supplementary Text). Thus, the superjogs are formed by multiple intersections with the lattice screw dislocations on the same glide plane. A single intersection results in the formation of kinks on the lattice screw dislocations and jogs on the grain boundary edge dislocations (or makes the jog length longer), as schematically shown in Fig. 6B. In addition to the geometric formation of the jogs and kinks after the intersections, the intermediate stage of the individual intersecting process can be investigated by detailed dislocation analyses. Figure 6C shows a dark-field TEM image of the same area as Fig. 6A, imaged using a (different) diffraction vector, $\mathbf{g} = \bar{2}\bar{1}1$. Under this imaging condition, the lattice screw dislocations, as well as the grain boundary edge dislocations, are visible, whereas the lattice screw dislocations are invisible under the conditions used in Fig. 6A. As indicated within the red rectangle, one lattice dislocation is trapped on the grain boundary plane, and it should be a screw dislocation that has been impeded at the end of the unloading process (see also the dislocation indicated by the red arrow in Fig. 5). By carefully inspecting the dislocation contrasts, the dislocation line is found to be imaged as a broken line. Compared with the dislocation contrasts in Fig. 6A, only the superjog segments are invisible in Fig. 6C. This indicates that the superjog segments should have a different Burgers vector from that of the grain boundary dislocations or that of the lattice dislocations. In addition, the Burgers vector of the superjog segments should be vertical to the direction of the diffraction vector, $\mathbf{g} = \bar{2}\bar{1}1$. Considering the dislocation reaction between the lattice dislocation (with the Burgers vector of $\mathbf{b}_{\mathrm{Lattice}}$) and the

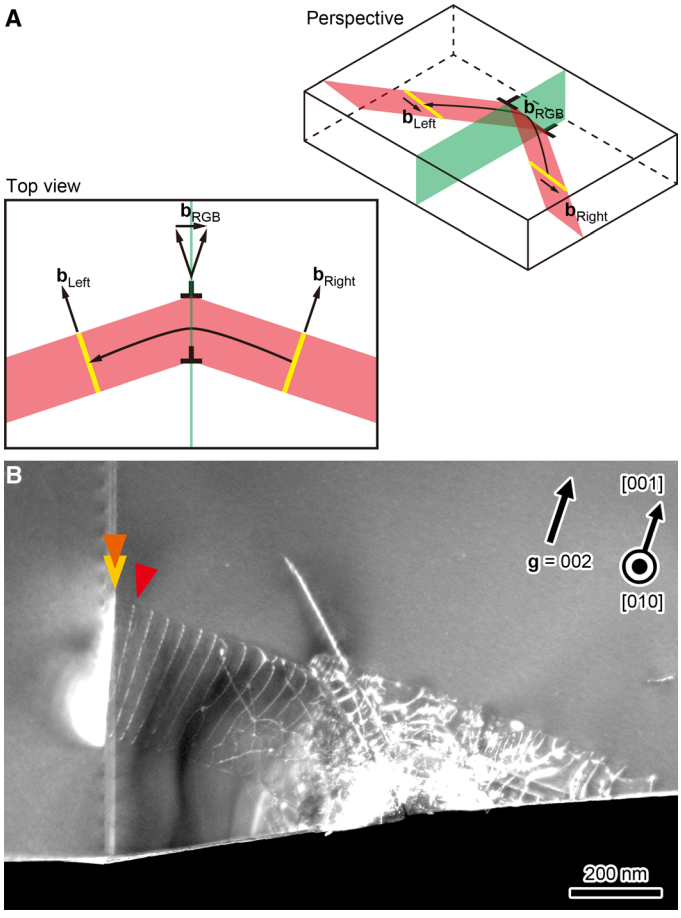

Fig. 3. Impediment mechanism of dislocation at the Σ5 grain boundary. (**A**) Schematic illustrations of the formation of a residual dislocation on a grain boundary when a dislocation is about to cross the boundary. If a lattice dislocation in the right crystal with the Burgers vector of $\mathbf{b}_{Right}$ crosses the grain boundary, the Burgers vector must be rotated into $\mathbf{b}_{Left}$. This results in the formation of a residual grain boundary dislocation with the Burgers vector of $\mathbf{b}_{RGB}$, which corresponds to the difference between that of the two lattice dislocations. (**B**) Dark-field TEM image after extracting the indenter tip. The first and second dislocations and the lower part of the third dislocation remain trapped on the grain boundary plane despite the intervals of other dislocations being relaxed because of the repulsive forces between them.

grain boundary dislocation ($\mathbf{b}_{GB}$), as schematically shown in Fig. 6D, the Burgers vector of the superjog segments ($\mathbf{b}_{Jog}$) should be

$$\mathbf{b}_{Jog} = \mathbf{b}_{Lattice} + \mathbf{b}_{GB} = [0\bar{1}1] + [100] = [1\bar{1}1]$$

This Burgers vector satisfies $\mathbf{g} \cdot \mathbf{b}_{Jog} = 0$ under the condition of $\mathbf{g} = \bar{2}\bar{1}1$. Therefore, the superjog segments must have a Burgers vector of $[1\bar{1}1]$. It is noted that this Burgers vector has a mixed dislocation character, whereas the lattice dislocations and the grain boundary dislocations have a pure screw and a pure edge character, respectively. The dislocation arrangement schematically illustrated in Fig. 6D can be considered as that of the intermediate stage of the intersecting processes (*33*). Thus, the lattice screw dislocations will partially become the mixed dislocations just on the grain boundary plane as a result of the dislocation reaction. On the basis of the above discussion, the schematic movie of the dynamic interaction process is given in the Supplementary Materials (movie S3).

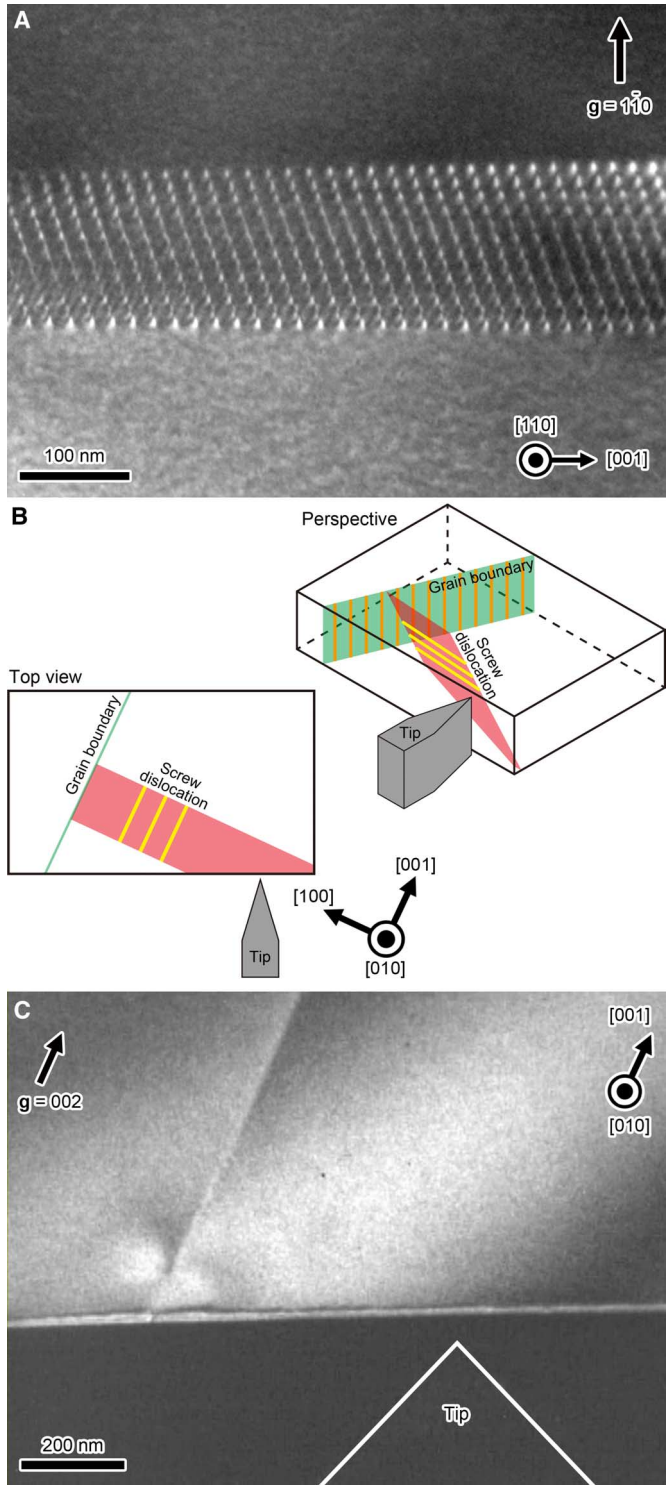

Fig. 4. TEM nanoindentation experiment with the low-angle tilt grain boundary. (**A**) Dark-field TEM image of the initial low-angle tilt grain boundary. The specimen was tilted from the edge-on condition to observe the grain boundary plane. The grain boundary consists of the periodic array of edge dislocations. (**B**) Schematic illustration of the geometric arrangement of the specimen, the grain boundary, the grain boundary edge dislocations, the indenter tip, and the introduced lattice screw dislocation. (**C**) Dark-field TEM image just before the nanoindentation experiment. The indenter tip was inserted at the direction of 25° off from the [001] direction for ease of dislocation propagation. The thickness of the specimen is about 150 nm.

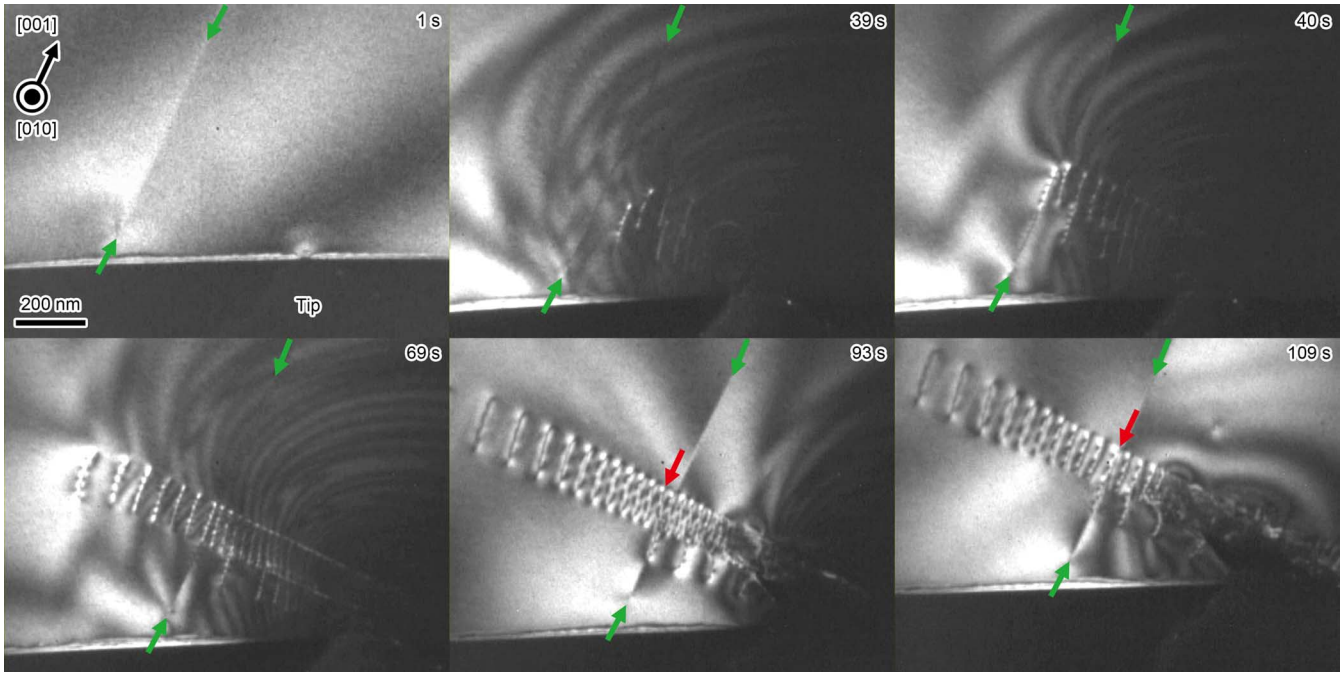

Fig. 5. Sequential TEM images captured from the movie of the nanoindentation experiment for the low-angle tilt grain boundary. Sequential dark-field TEM images captured from the movie recorded during the nanoindentation experiment. The green arrows in each image indicate the grain boundary position. In this experiment, the indenter tip was gradually inserted into the specimen edge from 0 to 85 s and extracted from 86 to 109 s. The introduced lattice dislocations propagated through the crystal and crossed the grain boundary into the adjacent crystal. In the unloading process, the lattice dislocations moved backward, and some dislocations crossed the grain boundary again and back into the initial crystal, where the grain boundary impeded the dislocation propagation. In the end, the dislocation indicated by the red arrow is impeded on the grain boundary plane.

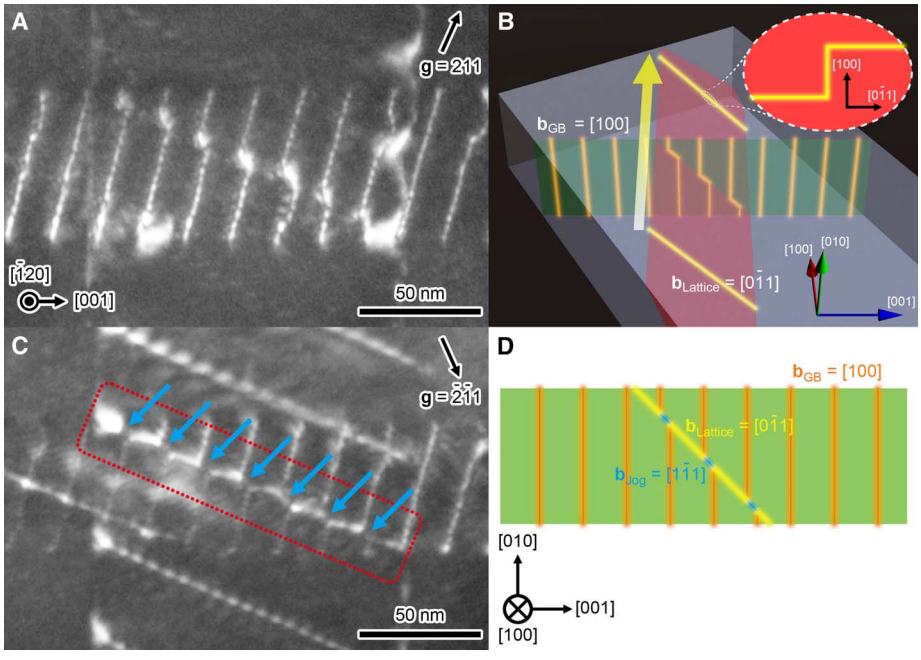

Fig. 6. Crossing mechanism of lattice screw dislocations across the low-angle tilt grain boundary. (**A**) Dark-field TEM image of the grain boundary edge dislocations after the nanoindentation experiment. Compared with Fig. 1B, it is clear that the grain boundary edge dislocation lines are shifted and the superjogs were formed on them. (**B**) Schematic illustration of the crossing process of the lattice screw dislocations. The intersection of the screw dislocation with the grain boundary edge dislocations forms the jogs on the grain boundary dislocations and the kinks on the lattice dislocation. (**C**) Dark-field TEM image of the same area shown in Fig. 3A, imaged with a different diffraction vector. The lattice dislocation within the red rectangle is trapped on the grain boundary plane. Only the superjog segments as indicated by the blue arrows are invisible, indicating that the Burgers vector of the superjog segments differs from that of the initial grain boundary edge dislocations. (**D**) Schematic illustration of the intermediate stage of screw dislocation crossing. The screw dislocation partially becomes mixed dislocations as a result of the dislocation reaction, $\mathbf{b}_{Jog} = \mathbf{b}_{Lattice} + \mathbf{b}_{GB}$.

Dislocation impediment mechanisms at low-angle grain boundary

Again, the low-angle tilt grain boundary slightly impeded the lattice screw dislocation motion not only when they crossed the grain boundary plane in the loading process but also when they moved back into the initial crystal grain during the unloading process. During the loading process, the intersection of the lattice screw dislocation with the grain boundary edge dislocations forms the jogs or lengthens the superjogs. This process corresponds to the formation of residual grain boundary dislocations in the high-angle grain boundary case, although the residual dislocations in the low-angle grain boundary case is the discrete (super)jog row (*32*). This means that the intersecting process during loading should lead to an increase in the self-energies of the grain boundary dislocations, consequently increasing the total energy. This may work as an effective energy barrier during the loading process to some extent. However, although the impediment of the lattice screw dislocation motion was also observed during the unloading process, the inverse intersection always shortened the length of the superjogs and thus led to a decrease in the self-energy. This observation strongly suggests the presence of other impediment mechanisms. Considering the fact that one screw dislocation was trapped on the grain boundary plane after removing the external stress, it can be concluded that the low-angle tilt grain boundary acts as a stable site for the lattice screw dislocations. As we have already discussed, the screw dislocations partially become the mixed dislocations when they react with the grain boundary dislocations at the intermediate stage of the intersections. It should be noted that this reaction will not increase the total elastic energy of the system (see Supplementary Text). Thus, the core relaxation induced by the dislocation reaction could be the main source of the stabilization at the grain boundary. This mechanism consistently explains the dislocation impediments during both loading and unloading processes. Our observations thus indicate that although there are almost no geometric discontinuities, low-angle grain boundaries impede dislocation glide at their cores by the stabilization of lattice dislocations.

DISCUSSION

Our direct and dynamic observations directly show the individual dislocation impediment processes at both high-angle and low-angle grain boundaries. The lattice dislocation impediment by grain boundaries does not simply originate from the geometric effects; it also arises as a result of local structural stabilization effects at their cores, especially in low-angle grain boundaries. The present findings indicate that both the geometric effects and the stabilization effects must be simultaneously considered to quantitatively understand the dislocation interaction processes at grain boundaries, required for a bottom-up approach to modeling the mechanical properties of polycrystalline materials. In situ TEM experiments with well-controlled samples are thus extremely powerful to fundamentally understand the dynamic and microscopic mechanisms of defect-defect interactions in various crystalline materials.

MATERIALS AND METHODS

Preparation of bicrystals and TEM specimens

The $SrTiO_3$ bicrystals, with the Σ5 grain boundary and the low-angle tilt grain boundary, were fabricated by diffusion bonding of two single crystals at 1500°C for 10 hours in air (Shinkosha Co. Ltd.). The specimens for the TEM nanoindentation were prepared as follows. The fabricated bicrystals were cut into small pieces and mechanically polished to a thickness of about 100 μm. They were then thinned to electron transparency by Ar^+ ion milling using an ion slicer (EM-09100IS, JEOL Ltd.) and an ion polishing system (Model 691, Gatan Inc.). From the TEM diffraction patterns from the grain boundary regions (see fig. S1), the misorientation angles of each grain boundary were estimated to be 36.9° and 1.2°, which correspond to the misorientation angle of the Σ5 grain boundary and the low-angle tilt grain boundary, respectively.

In situ TEM nanoindentation experiments

The in situ TEM observations were performed using a JEM-2010 transmission electron microscope (JEOL Ltd.) operated at 200 kV. This TEM is equipped with a double-tilt TEM-nanoindenter holder (Nanofactory Instruments AB), which enables nanoindentation experiments inside a transmission electron microscope. The indentation mechanics consist of a fixed indenter tip and a movable specimen that is precisely controlled by a piezo actuator. During the in situ observations, the specimen was manually moved toward the fixed indenter tip with the speed of a few nanometers per second. The sequential TEM images were recorded as a movie with a frame rate of 30 fps using a video camera for TEM and a video recorder (SR-DVM700, Victor Ltd.). Details of the in situ TEM nanoindentation system have been reported elsewhere (*21*).

SUPPLEMENTARY MATERIALS

Supplementary material for this article is available at http://advances.sciencemag.org/cgi/content/full/2/11/e1501926/DC1

Supplementary Text

fig. S1. TEM diffraction patterns obtained from the grain boundary region.

fig. S2. Bright-field and dark-field TEM images of the introduced dislocations by nanoindentation for the Σ5 grain boundary.

fig. S3. Bright-field and dark-field TEM images of the introduced dislocations within the low-angle tilt grain boundary specimen.

fig. S4. Dark-field TEM images captured during TEM nanoindentation for the Σ5 grain boundary.

fig. S5. Number of the trapped dislocations on the Σ5 grain boundary after nanoindentation.

fig. S6. Dark-field TEM image of the Σ5 grain boundary plane after nanoindentation.

fig. S7. Dark-field TEM images for the **g**·**b** contrast analyses of the trapped dislocations on the Σ5 grain boundary.

fig. S8. Bright-field TEM image of dislocation configuration after nanoindentation for the low-angle tilt grain boundary.

movie S1. Experimental TEM movie of the in situ nanoindentation experiment for the Σ5 grain boundary.

movie S2. Experimental TEM movie of the in situ nanoindentation experiment for the low-angle tilt grain boundary.

movie S3. Schematic movie showing the interaction process of lattice screw dislocations with the low-angle tilt grain boundary.

References (*34*–*37*)

REFERENCES AND NOTES

1. J. P. Hirth, J. Lothe, *Theory of Dislocations* (Krieger Publishing Company, ed. 2, 1992).
2. J. P. Hirth, The influence of grain boundaries on mechanical properties. *Metall. Trans.* **3**, 3047–3067 (1972).
3. L. Priester, *Grain Boundaries* (Springer, 2013).
4. J. Kacher, B. P. Eftink, B. Cui, I. M. Robertson, Dislocation interactions with grain boundaries. *Curr. Opin. Solid State Mater. Sci.* **18**, 227–243 (2014).
5. E. O. Hall, The deformation and ageing of mild steel: III Discussion of results. *Proc. Phys. Soc. B* **64**, 747–753 (1951).
6. N. J. Petch, The cleavage strength of polycrystals. *J. Iron Steel Inst.* **174**, 25–28 (1953).
7. J. D. Eshelby, F. C. Frank, F. R. N. Nabarro, The equilibrium of linear arrays of dislocations. *Philos. Mag.* **42**, 351–364 (1951).
8. R. W. Armstrong, Dislocation pile-ups: From {1 1 0} cracking in MgO to model strength evaluations. *Mater. Sci. Eng. A* **409**, 24–31 (2005).

9. L. C. Lim, R. Raj, Continuity of slip screw and mixed crystal dislocations across bicrystals of nickel at 573 K. *Acta Metall.* **33**, 1577–1583 (1985).
10. J. D. Livingston, B. Chalmers, Multiple slip in bicrystal deformation. *Acta Metall.* **5**, 322–327 (1957)
11. Z. Shen, R. H. Wagoner, W. A. T. Clark, Dislocation pile-up and grain boundary interactions in 304 stainless steel. *Scripta Metall.* **20**, 921–926 (1986).
12. A. K. Head, The interaction of dislocations and boundaries. *Philos. Mag.* **44**, 92–94 (1953).
13. A. K. Head, Edge dislocations in inhomogeneous media. *Proc. Phys. Soc. B* **66**, 793–801 (1953).
14. D. M. Barnett, J. Lothe, An image force theorem for dislocations in anisotropic bicrystals. *J. Phys. F* **4**, 1618–1635 (1974).
15. Z. Shen, R. H. Wagoner, W. A. T. Clark, Dislocation and grain boundary interactions in metals. *Acta Metall.* **36**, 3231–3242 (1988).
16. Y. Ikuhara, T. Suzuki, Y. Kubo, Transmission electron microscopy in situ observation of crack propagation in sintered alumina. *Philos. Mag. Lett.* **66**, 323–327 (1992).
17. S. H. Oh, M. Legros, D. Kiener, G. Dehm, In situ observation of dislocation nucleation and escape in a submicrometre aluminium single crystal. *Nat. Mater.* **8**, 95–100 (2009).
18. D. Kiener, P. Hosemann, S. A. Maloy, A. M. Minor, In situ nanocompression testing of irradiated copper. *Nat. Mater.* **10**, 608–613 (2011).
19. A. M. Minor, S. A. S. Asif, Z. Shan, E. A. Stach, E. Cyrankowski, T. J. Wyrobek, O. L. Warren, A new view of the onset of plasticity during the nanoindentation of aluminium. *Nat. Mater.* **5**, 697–702 (2006).
20. J. T. M. De Hosson, W. A. Soer, A. M. Minor, Z. Shan, E. A. Stach, S. A. S. Asif, O. L. Warren, In situ TEM nanoindentation and dislocation-grain boundary interactions: A tribute to David Brandon. *J. Mater. Sci.* **41**, 7704–7719 (2006).
21. S. Kondo, N. Shibata, T. Mitsuma, E. Tochigi, Y. Ikuhara, Dynamic observations of dislocation behavior in $SrTiO_3$ by in situ nanoindentation in a transmission electron microscope. *Appl. Phys. Lett.* **100**, 181906 (2012).
22. J. P. Buban, K. Matsunaga, J. Chen, N. Shibata, W. Y. Ching, T. Yamamoto, Y. Ikuhara, Grain boundary strengthening in alumina by rare earth impurities. *Science* **311**, 212–215 (2006).
23. N. Shibata, S. D. Findlay, S. Azuma, T. Mizoguchi, T. Yamamoto, Y. Ikuhara, Atomic-scale imaging of individual dopant atoms in a buried interface. *Nat. Mater.* **8**, 654–658 (2009).
24. Z. Wang, M. Saito, K. P. McKenna, L. Gu, S. Tsukimoto, A. L. Shluger, Y. Ikuhara, Atom-resolved imaging of ordered defect superstructures at individual grain boundaries. *Nature* **479**, 380–383 (2011).
25. V. Ravikumar, V. P. Dravid, Atomic structure of undoped $\Sigma = 5$ symmetrical tilt grain boundary in strontium titanate. *Ultramicroscopy* **52**, 557–563 (1993).
26. M. Imaeda, T. Mizoguchi, Y. Sato, H.-S. Lee, S. D. Findlay, N. Shibata, T. Yamamoto, Y. Ikuhara, Atomic structure, electronic structure, and defect energetics in [001](310)Σ5 grain boundaries of $SrTiO_3$ and $BaTiO_3$. *Phys. Rev. B* **78**, 245320 (2008).
27. D. B. Williams, C. B. Carter, *Transmission Electron Microscopy* (Springer, ed. 2, 2009).
28. L. Priester, On the accommodation of extrinsic dislocations in grain boundaries. *Interface Sci.* **4**, 205–219 (1997).
29. A. P. Sutton, R. W. Balluffi, *Interfaces in Crystalline Materials* (Oxford Univ. Press, 1995).
30. Z. Zhang, W. Sigle, M. Rühle, Atomic and electronic characterization of the *a*[100] dislocation core in $SrTiO_3$. *Phys. Rev. B* **66**, 094108 (2002).
31. J. P. Buban, M. Chi, D. J. Masiel, J. P. Bradley, B. Jiang, H. Stahlberg, N. D. Browning, Structural variability of edge dislocations in a $SrTiO_3$ low-angle [001] tilt grain boundary. *J. Mater. Res.* **24**, 2191–2199 (2009).
32. J. P. Hirth, R. C. Pond, J. Lothe, Spacing defects and disconnections in grain boundaries. *Acta Mater.* **55**, 5428–5437 (2007).
33. C. B. Carter, P. B. Hirsch, The formation and glide of jogs in low stacking-fault energy face-centred cubic materials. *Philos. Mag.* **35**, 1509–1522 (1977).
34. P. Hirel, M. Mrovec, C. Elsässer, Atomistic simulation study of <1 1 0> dislocations in strontium titanate. *Acta Mater.* **60**, 329–338 (2012).
35. O. Khalfallah, M. Condat, L. Priester, H. O. K. Kirchner, Image effects between dislocations and grain boundaries. *Philos. Mag. A* **61**, 291–304 (1990).
36. P. Gumbsch, S. Taeri-Baghbadrani, D. Brunner, W. Sigle, M. Rühle, Plasticity and an inverse brittle-to-ductile transition in strontium titanate. *Phys. Rev. Lett.* **87**, 085505 (2001).
37. D. Brunner, Low-temperature plasticity and flow-stress behaviour of strontium titanate single crystals. *Acta Mater.* **54**, 4999–5011 (2006).

Acknowledgments: We thank N. Lugg for carefully reading our manuscript. **Funding:** A part of this work was supported by the Elements Strategy Initiative for Structural Materials from the Ministry of Education, Culture, Sports, Science and Technology in Japan (MEXT); the "Nanotechnology Platform" (project no. 12024046) by MEXT; and a Grant-in-Aid for Scientific Research (A) (grant no. 15H02290) from the Japan Society for the Promotion of Science (JSPS). S.K. acknowledges support by the JSPS Research Fellowship for Young Scientists (grant no. 13J04234). N.S. acknowledges support from a Grant-in-Aid for Scientific Research on Innovative Areas "Nano Informatics" (grant no. 25106003) from JSPS. **Author contributions:** S.K. carried out the TEM experiments and wrote the paper. T.M. designed and supported the experiments. N.S. wrote the paper. Y.I. directed the entire study. **Competing interests:** The authors declare that they have no competing interests. **Data and materials availability:** All data needed to evaluate the conclusions in the paper are present in the paper and/or the Supplementary Materials. Additional data related to this paper may be requested from the authors.

Submitted 30 December 2015
Accepted 11 October 2016
Published 11 November 2016
10.1126/sciadv.1501926

Citation: S. Kondo, T. Mitsuma, N. Shibata, Y. Ikuhara, Direct observation of individual dislocation interaction processes with grain boundaries. *Sci. Adv.* **2**, e1501926 (2016).